Supporting Information

for

Catalytic N-N Coupling of Aryl Azides to Yield Azoarenes via TBP Fe-Nitrene Intermediates

Neal P. Mankad, Peter Müller, and Jonas C. Peters

Experimental Section.

General Considerations. All manipulations were carried out using standard Schlenk or glovebox techniques under a N_2 atmosphere unless otherwise indicated. Unless otherwise noted, solvents were deoxygenated and dried by thoroughly sparging with Ar gas followed by passage through an activated alumina column in the solvent purification system by SG Water, USA LLC. Non-halogenated solvents were tested with a standard purple solution of sodium benzophenone ketyl in tetrahydrofuran in order to confirm effective oxygen and moisture removal. $[SiP^{iPr}_3]Fe(N_2)$ (**1**) was prepared according to literature procedures.[1] LiNHTol was prepared from NH_2Tol and *n*BuLi in *n*-pentane. All aryl azides were prepared according to literature procedures.[2] All azoarene and carbodiimide products were synthesized independently by literature methods to compare characterization data.[3,4] All other reagents were purchased from commercial vendors and used without further purification. Elemental analyses were performed by Midwest Microlab, LLC, Indianapolis, IN. Deuterated solvents were purchased from Cambridge Isotope Laboratories, Inc., degassed, and dried over activated 3-Å molecular sieves prior to use. Photolysis was conducted with a Blak-Ray long-wave UV, medium skirted Hg spot lamp (100 W).

X-ray Crystallography. Low-temperature diffraction data were collected on a Siemens Platform three-circle diffractometer coupled to a Bruker-AXS Smart Apex CCD detector with graphite-monochromated Mo Kα radiation (λ = 0.71073 Å), performing ϕ-and ω-scans. The

structures were solved by direct methods using SHELXS[5] and refined against F^2 on all data by full-matrix least squares with SHELXL-97[6] using established methods[7]. All non-hydrogen atoms were refined anisotropically. All hydrogen atoms (except the hydrogen on nitrogen atom N in the structure of **6**, which was taken from the difference Fourier synthesis and refined semi-freely with the help of distance restraints) were included into the model at geometrically calculated positions and refined using a riding model. The isotropic displacement parameters of all hydrogen atoms were fixed to 1.2 times the *U* value of the atoms they are linked to (1.5 times for methyl groups). Details of the data quality and a summary of the residual values of the refinements are listed in tables S9 and S10 below.

Compound **6** crystallizes in the orthorhombic space group $P2_12_12_1$ with one molecule per asymmetric unit. Structure solution and refinement were straightforward and routine. Compound **2** crystallizes in the rhombohedral space group *R*-3*c* (hexagonal setting) with one third of **2** plus one half of an *n*-pentane molecule per asymmetric unit. Only parts of the molecule of **2** show threefold symmetry, which results in a threefold disorder of the 1-adamantylazide moiety about the crystallographic threefold axis. The half solvent molecule is disordered over four positions involving a crystallographic twofold axis; hence only two of the four positions are crystallographically independent, corresponding to one half pentane molecule in the asymmetric unit. The ratio between the two independent components of the solvent disorder was refined freely and converged at 0.710(8). Similarity restraints on 1-2 and 1-3 distances and displacement parameters as well as rigid bond restraints for anisotropic displacement parameters were applied to all atoms of the solvent molecule and also of the adamantyl moiety. The fact that the asymmetric unit contains one third of **2** but one half pentane molecule results in a non-integer number for the element C in the empirical formula.

Spectroscopic measurements. Varian Mercury-300 and Inova-500 spectrometers were used to record ^{1}H, ^{19}F, and ^{31}P NMR spectra at ambient temperature unless otherwise indicated. ^{1}H chemical shifts were referenced to the residual solvent peaks. ^{19}F chemical shifts were referenced to external hexafluorobenzene ($\delta = -165$ ppm). ^{31}P chemical shifts were referenced to external phosphoric acid ($\delta = 0$ ppm). Solution magnetic moments were determined by the method of Evans.[8,9] Optical spectroscopy measurements were taken on a Cary 50 UV-Vis spectrophotometer using either a 1-cm or 2-mm two-window quartz cell sealed with a standard closed cap purchased from Starna Cells, Inc. Infrared spectra were recorded on a BioRad FTS 3000 EXCALIBUR series FT-IR spectrometer. An Agilent 5973N Gas Chromatograph/Mass Spectrometer was used for GC-MS analysis. X-band EPR measurements were recorded using a Brüker EMX spectrometer at 77 K in 2-methyltetrahydrofuran glasses. EPR samples were prepared in a glovebox under N_2 in quartz EPR tubes equipped with J. Young caps. X-band microwave frequencies: [SiP$^{iPr}_3$]Fe(N_2), ν = 9.3368 GHz; [SiP$^{iPr}_3$]Fe(η^1-N_3Ad), ν = 9.3367 GHz; [SiP$^{iPr}_3$]Fe(N_3Tol), ν = 9.3379 GHz, [SiP$^{iPr}_3$]Fe(NTol), ν = 9.3761 GHz. Microwave power: 2.0 mW. Modulation amplitute: 10.0 G. Time constant: 2.56 ms. Data collection parameters: 1024 data points, 10 scans. EPR spectra were simulated using the W95EPR program.[10]

Synthetic procedures.

Synthesis of [SiP$^{iPr}_3$]Fe(η^1-N_3Ad) (2). A solution of 1-adamantylazide (31.6 mg, 0.178 mmol) in benzene (3 mL) was added to solid **1** (78.0 mg, 0.113 mmol), resulting in effervescence and a darkening of the solution. The brown solution was stirred for 6 days, and then volatiles were removed *in vacuo*. *n*-Pentane (1 mL) was added, and the resulting brown insoluble material was collected on a sintered glass frit and washed with additional *n*-pentane (2 x 1 mL). The solids were then lyophilized from benzene to give **2** as a brown powder (54.3 mg, 57%). X-ray quality crystals were grown by diffusion of hexamethyldisiloxane vapors into a pentane solution of **2**. In the absence of excess 1-adamantylazide, a trace equilibrium amount of **1** was consistently evident by ^{1}H NMR spectroscopy. Therefore, combustion analysis was not obtained. ^{1}H NMR (C_6D_6, δ): 11.4, 7.3, 7.0, 6.8, 3.9, 2.0, 1.8-1.0 (multiple overlapping peaks), 0.4, 0.3, -6.6. IR (KBr pellet, cm^{-1}): 2086 (ν_{N3}). μ_{eff} (C_6D_6, room temp): 2.2 μ_B. UV-Vis (C_6H_6, nm(M^{-1}cm^{-1})): 298(37000), 406(11000), 679(1100).

Synthesis of [SiP$^{iPr}_3$]Fe(CN^{t}Bu) (5). Addition of *tert*-butylisocyanide (2.03 μL, 0.0179 mmol) to a solution of **1** (12.4 mg, 0.0179 mmol) in benzene-d_6 (~0.7 mL) provided **5** *in situ* after stirring for 18 h. In the absence of excess isocyanide, complex **1** was consistently a minor impurity in the product mixtures. Moreover, prolonged exposure of these solutions to vacuum caused the majority of the material to revert to **1** upon re-exposure to an N_2 atmosphere, as judged by ^{1}H NMR. Therefore, complex **5** was not isolated in pure form; characterization data for **5** generated *in situ* is provided here and match the data obtained from the competitive trapping experiments (*vide infra*). ^{1}H NMR (C_6D_6, δ): 10.3, 6.8, 4.9, 4.3, 1.6, 0.9. IR (C_6D_6 solution, cm^{-1}): 1977 (ν_{CN}).

Synthesis of [SiP$^{iPr}_3$]Fe(OTf). Complex **1** (0.565 g, 0.817 mmol) was dissolved in THF

(10 mL) and frozen in a cold well bathed in liquid N_2. Silver triflate (0.211 g, 0.821 mmol) was dissolved in THF (5 mL) and likewise frozen. As the silver triflate solution thawed, it was added dropwise to the still-frozen solution of **1**. The entire mixture was then allowed to thaw and warm to room temperature, resulting in a darkening of the solution and precipitation of black solids. After stirring at room temperature for 2 h, the mixture was filtered through Celite and evaporated to dryness. A toluene/*n*-pentane mixture (1:1, 10 mL) was added, the resulting solution was filtered once again, and the dark orange filtrate was placed in a -35°C freezer overnight, resulting in light orange crystals of [SiP$^{iPr}_3$]Fe(OTf) (0.397 g, 60%). ^{1}H NMR (C_6D_6, δ): 31.7, 6.8, 6.6, 5.4, 1.8, 1.0, -0.4, -4.8. ^{19}F NMR (C_6D_6, δ): -55.6 (br). IR (KBr pellet, cm^{-1}): 3039, 2956, 2922, 2870, 1496, 1424, 1383, 1367, 1315, 1226, 1207, 1174, 1106, 1019. μ_{eff} (C_6D_6, room temp): 2.8 μ_B. UV-Vis (C_6H_6, nm(M^{-1}cm^{-1})): 367(4700), 427(5400), 486(6900). Anal. Calcd for $C_{37}H_{54}F_3FeO_3P_3SSi \cdot C_7H_8$ ([SiP$^{iPr}_3$]Fe(OTf)·toluene): C, 58.40; H, 6.91. Found: 58.49, 6.68.

Synthesis of [SiP$^{iPr}_3$]Fe(NHTol) (6). A thawing solution of LiNHTol (21.5 mg, 0.190 mmol) in THF (1 mL) was added to a frozen solution of [SiP$^{iPr}_3$]Fe(OTf) (0.149 g, 0.183 mmol). The mixture was allowed to warm to room temperature gradually, resulting a color change to an intense cherry red. After stirring for 18 h at room temperature, volatiles were removed *in vacuo*. *n*-Pentane (10 mL) was added, and the resulting solution was filtered. The cherry red filtrate was concentrated *in vacuo* to red solids (93.3 mg, 66%). ^{1}H NMR of this material indicates that the product contains **1** and NH_2Tol as minor impurities. Recrystallization from *n*-pentane (-35°C or by slow evaporation) gave red crystals of co-crystallized **6** and **1**, and these complexes could not be separated in our hands by repeated crystallization. X-ray quality crystals were grown by diffusion of hexamethyldisiloxane vapors into a pentane solution of crude **6**, and a crystal of **6** rather than **1** was selected based upon color. Crude characterization with only spectral data

attributed to **6** is presented here. ^{1}H NMR (C_6D_6, δ): 87, 38, 5.6, -0.6, -1.5, -2.7. IR (C_6H_6 solution, cm^{-1}): 3380 (ν_{NH}).

Catalytic conversion of aryl azides to azoarenes.

General procedure. Catalyst **1** was dissolved in a solvent (approx 1 mL) in a resealable Schlenk tube equipped with a stirbar. The aryl azide and an internal integration standard (mesitylene or $FeCp_2$) were added, and the resulting solution was sealed and stirred as indicated in Table S1. The solution color progressed from red to brown to green to brown to red, at which point the reaction was complete as judged by full consumption of starting azide based on separate *in situ* NMR experiments. Yields of azoarene and aniline were determined by ^{1}H NMR analysis (integration against the internal standard). IR spectroscopy of the solutions confirmed the presence of **1**. Filtration through silica gel under air followed by analysis by GC-MS confirmed the product assignments. ^{1}H NMR and GC-MS characterization of the azoarene products were reproduced with authentic samples prepared by literature methods.[3] A representative NMR spectrum is shown in Figure S1. Tabulated results are presented in Table S1. In two cases, yields were confirmed by quantitative GC-MS analysis.

Generation of unsymmetrical diazo products.

The product profile resulting from mixing **3-Tol** and **2** contains **1**, **2**, TolN=NTol, $TolNH_2$, and trace AdN=NTol. The ratio of TolN=NTol to AdN=NTol is estimated to be 5:1. One possible pathway to form AdN=NTol is the reaction between intermediate **4-Tol** and **2**, especially because AdN=NTol does not result from mixing **3-Tol** and free AdN_3. Likewise, in addition to the proposed bimolecular coupling of **4-Tol**, a second possible pathway to form

TolN=NTol is the reaction between intermediate **4-Tol** and **3-Tol**. However, we still believe that bimolecular coupling of **4-Tol** is the dominant N-N coupling pathway for two reasons: 1) In the absence of **2**, **3-Tol** would not decay cleanly with first-order kinetics as observed if reaction between **4-Tol** and **3-Tol** were occurring to a significant extent; 2) a TolN=NTol:AdN=NTol ratio closer to 1:1 is expected if **4-Tol** reacts with either azide adduct **3-Tol** or **2** rapidly relative to bimolecular coupling of **4-Tol**. For comparison, mixing equimolar **3-Ph** and **3-Tol** gives PhN=NPh, PhN=NTol, and TolN=NTol in a 1:2:1 ratio.

Table S1. Results from the catalytic decomposition of aryl azides (N_3Ar) by catalyst **1**.

Entry	Ar	Temp. (°C)	Solvent	Catalyst Loading (%)	Reaction Time (h)	Yield ArNNAr (%)	Yield $ArNH_2$ (%)
1	*p*-tolyl	23	Benzene	10	48	46	5
2	*p*-tolyl	45	Benzene	5	17	52	11
3	*p*-tolyl	70	Benzene	5	3	57	8
4	*p*-tolyl	70	Benzene	0	17	0	0
5	*p*-tolyl	70	C_7H_{14}	5	18[a]	25	< 2
6	*p*-tolyl	70	THF	5	18[a]	10	< 2
7	Ph	70	Benzene	5	18[a]	44	24
8	*p*-C_6H_4OMe	70	Benzene	5	18[a]	50	16
9	Mes	70	Benzene	5	18[a]	50	22
10	Ph	23	Benzene	100	18	36	0
11	*p*-tolyl	23	Benzene	100	18	48	0
12	*p*-C_6H_4OMe	23	Benzene	100	18	46	0
13	Mes	23	Benzene	100	18	19	0

[a] Separate *in situ* NMR experiments established that reaction times of < 3 h were sufficient for these conditions.

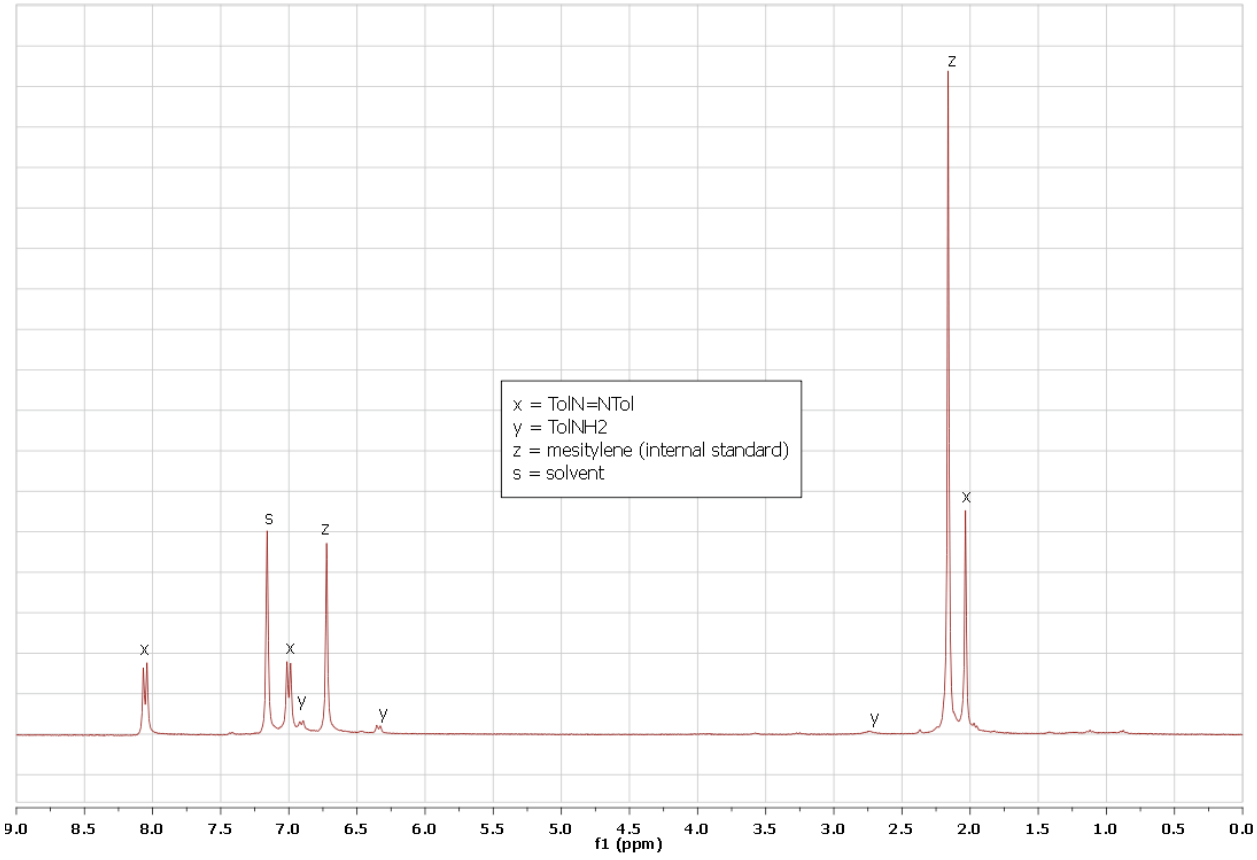

Figure S1. ^{1}H NMR spectrum from the catalytic decomposition of N_3Tol by catalyst **1**.

IR data for [SiP$^{iPr}_3$]Fe(N$_3$Ar).

General procedure. [SiP$^{iPr}_3$]Fe(N$_2$) was dissolved in benzene, and an aryl azide (1 equiv) was added. Periodically, aliquots were transferred to a solution IR cell and analyzed by IR spectroscopy. Representative spectra are presented in Figure S2. In all cases, the difference between free and coordinated azide was found to be $\Delta\nu(N_3) \leq 2$ cm^{-1} (see Table S2).

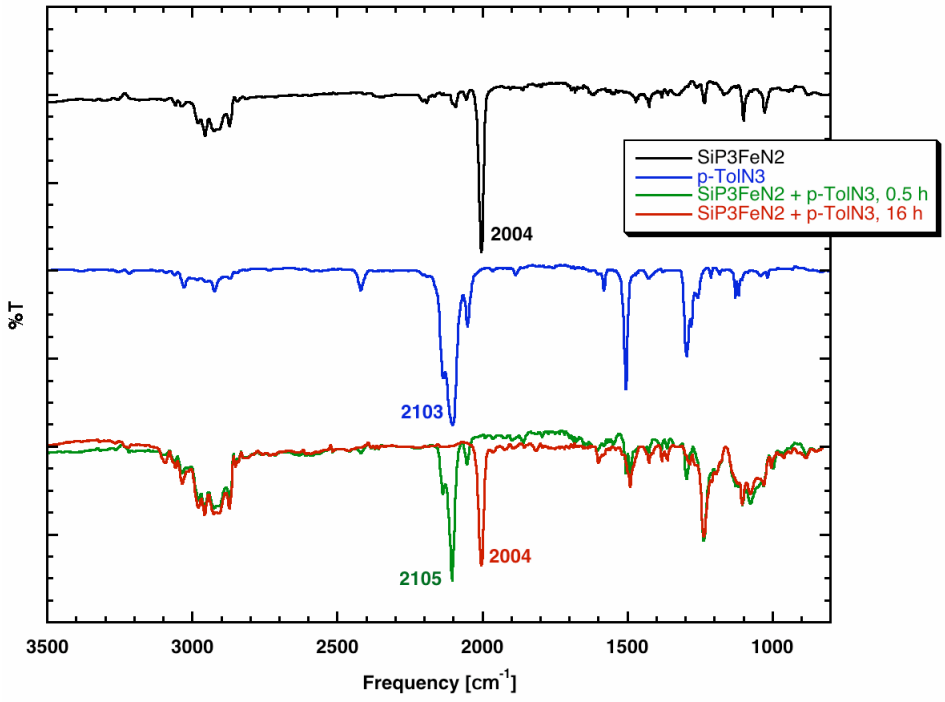

Figure S2. IR spectra (benzene solutions) of **1**, TolN$_3$, and initial and final time points for the reaction between **1** and TolN$_3$.

Table S2. IR data for various [SiP$^{iPr}_3$]Fe(N$_3$Ar) derivatives in benzene solution.

Ar	$\nu(N_3)$ (cm^{-1})	$\nu(N_3)$ (cm^{-1}) (free azide)
Ph	2127	2127
p-tolyl	2105	2103
p-C$_6$H$_4$OMe	2104	2104
Mes	2120	2119
2,6-Et$_2$C$_6$H$_3$	2098	2098

UV-Vis Spectroscopy and Kinetics.

General procedures. All UV-Vis spectra were recorded in benzene solution. Figure S3 shows spectra for the various [SiP$^{iPr}_3$]Fe(N$_3$Ar) derivatives as well as complexes **1** and **2** recorded at arbitrary concentrations in a 1-cm path length cell.

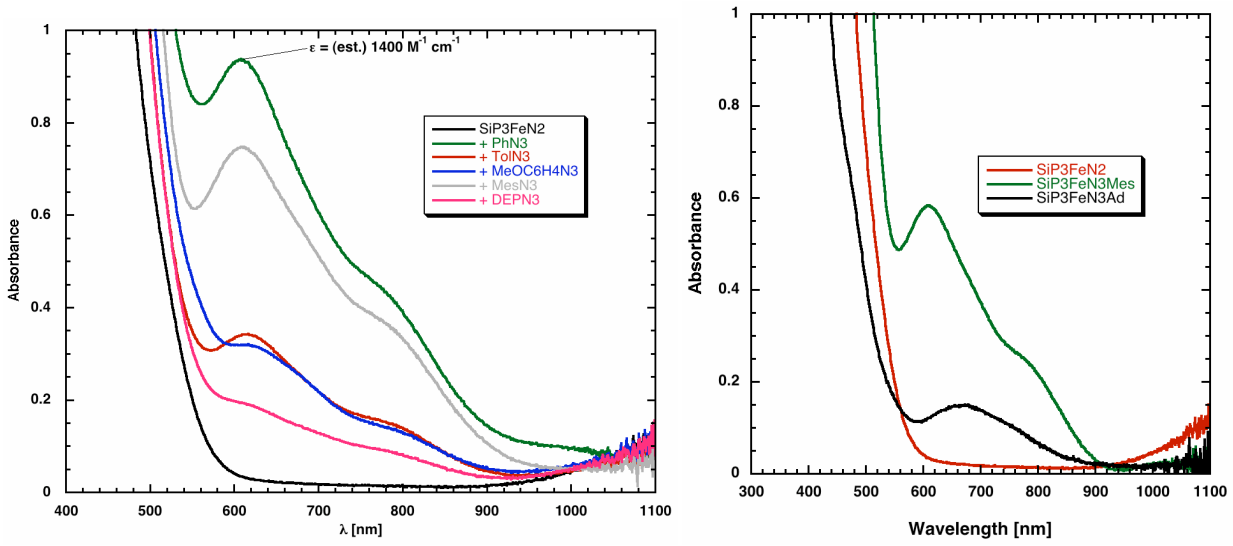

Figure S3. (*left*) UV-Vis spectra of various [SiP$^{iPr}_3$]Fe(N$_3$Ar) derivatives at arbitrary concentrations in benzene solutions. (*right*) Overlain UV-Vis spectra of [SiP$^{iPr}_3$]Fe(N$_2$) (**1**), [SiP$^{iPr}_3$]Fe(η^1-N$_3$Ad) (**2**), and [SiP$^{iPr}_3$]Fe(N$_3$Mes).

UV-Vis Kinetics. The decay rates of the various [SiP$^{iPr}_3$]Fe(N$_3$Ar) species were monitored at room temperature in 2-mm path length cells. In each experiment, a stock solution of complex **1** (3.3 mM) was loaded into the cell, and then 1 equiv of the aryl azide was added. Data points were taken every 15 min. Over the earliest data points, the peaks corresponding to the green intermediate species (see Figure S3) were observed to be growing in. During the many subsequent data points, these peaks proceeded to decay. The kinetic analysis of the disappearance of the green intermediates was based upon the latter set of points. An example of this decaying absorbance is shown in the main text in Figure 2. Isosbestic points are evident in Figure 2 and were evident in for all aryl groups canvassed. Plots of ln(A_t/A_0) versus time

revealed linear relationships ($R > 0.99$) in all cases, indicating first order processes. An example of such a plot is shown in the main text in Figure 2. The first-order rate constants were extracted from the slopes of these linear plots, and the half-lives tabulated in Table S3 are based upon those rate constants. The linearities and slopes of the lines were independent of wavelength, and the half-lives in Table S3 are based upon decay at the λ_{max} of each species that is near 610 nm (Table S3).

Table S3. λ_{max} and half life data for $[SiP^{iPr}_3]Fe(N_3R)$ at room temperature in C_6H_6 solution.

R	**λ_{max} (nm)**	**$t_{1/2}$ (h)**
Ph	608	1.3
p-tolyl	614	1.8
p-C_6H_4OMe	617	3.2
Mes	609	1.2
2,6-$Et_2C_6H_3$	617	2.2
1-adamantyl	679	N/A

EPR Spectroscopy.

General procedures. EPR spectra were recorded in 2-methyltetrahydrofuran glasses (~ 5-10 mM) at 77 K. In the cases of **1** and **2**, isolated material was utilized to record the spectra. In the case of [SiP$^{iPr}_3$]Fe(N_3Tol), complex **1** was incubated with N_3Tol in 2-methyltetrahydrofuran for 0.5 h prior to freezing. Optical spectroscopy was used to determine that this was the optimal amount of time to maximize concentration of **3-Tol** and minimize the concentration of residual **1**. Figures S4 – S7 present EPR data and fits, and Table S4 summarizes the resulting EPR parameters.

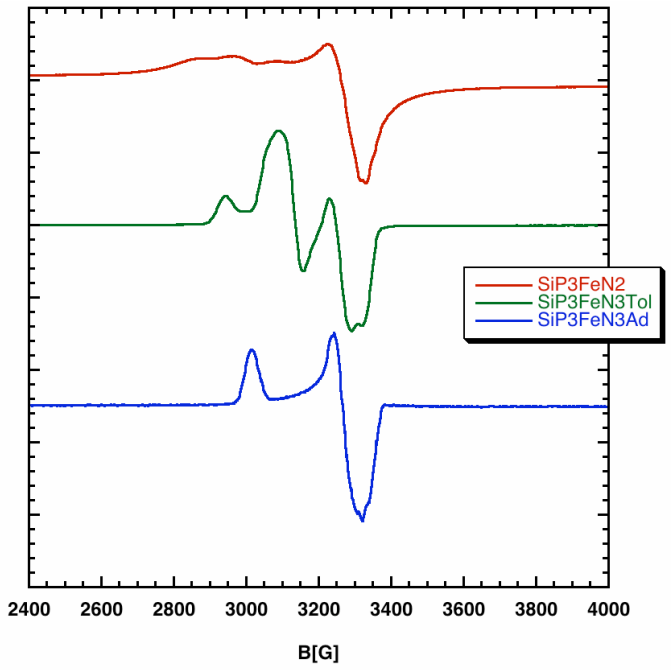

Figure S4. X-band EPR spectra (2-methyltetrahydrofuran glass, 77 K) of isolated **1** and **2**, as well as [SiP$^{iPr}_3$]Fe(N_3Tol) generated *in situ*.

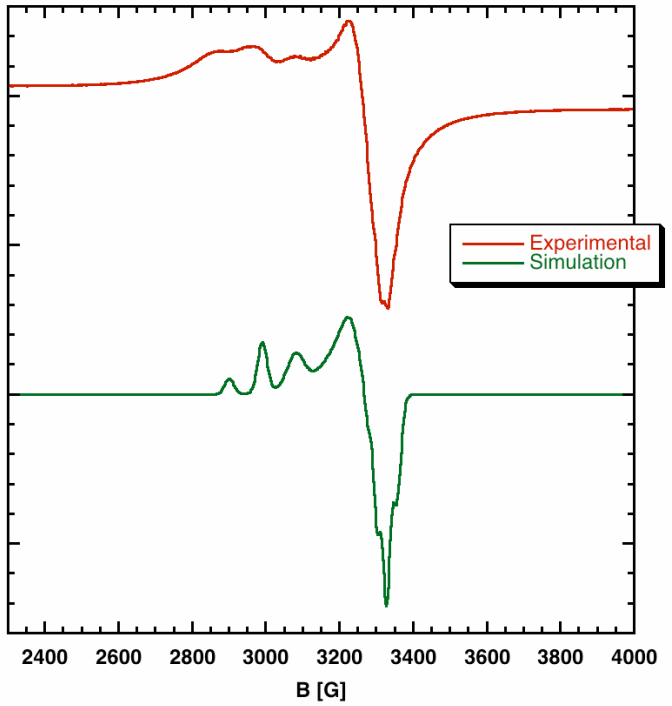

Figure S5. Experimental (red) and simulated (green) EPR spectra for complex **1**.

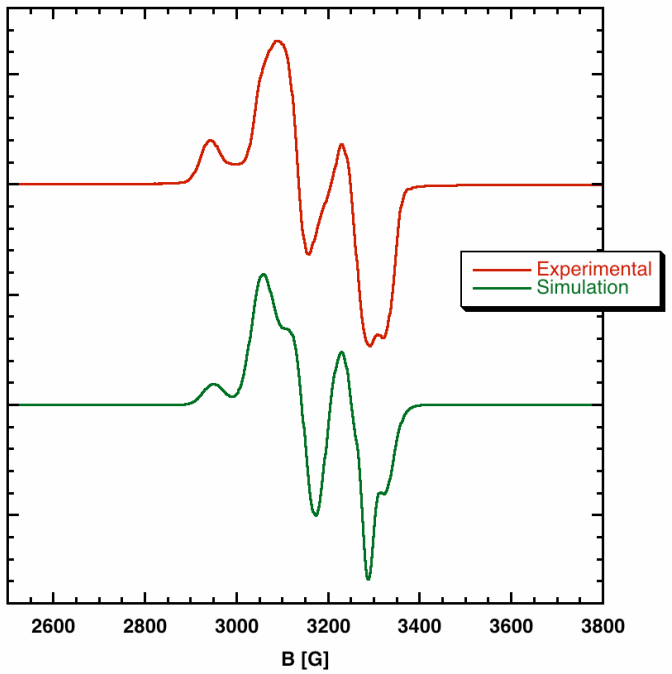

Figure S6. Experimental (red) and simulated (green) EPR spectra for *in situ* generated [SiP^{iPr}_3]Fe(N_3Tol).

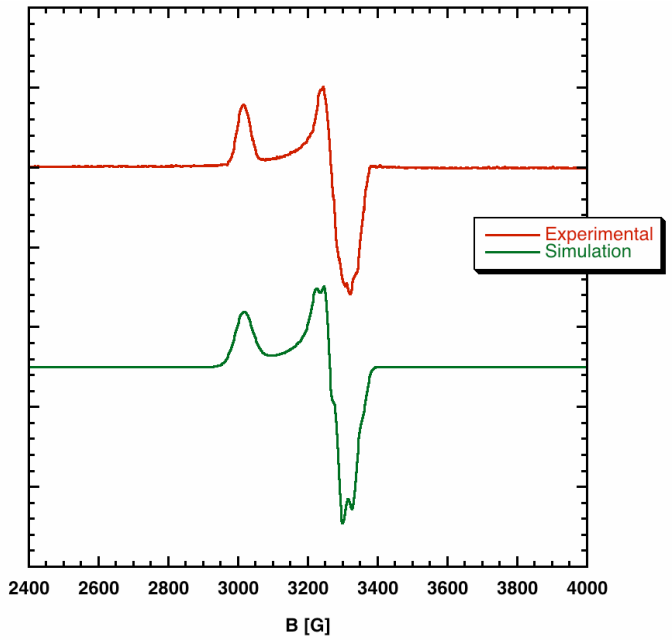

Figure S7. Experimental (red) and simulated (green) EPR spectra for complex **2**.

Observation of the EPR spectrum for [SiP$^{iPr}_3$]Fe(NTol). Complex **1** (15.6 mg, 0.0226 mmol) was dissolved in 2-methyltetrahydrofuran (1.00 mL) and split into two equal solutions (A and B). To solution A was added *p*-tolylazide (1.27 µL, 0.0113 mmol). After 1 h an aliquot from the resulting deep green Solution A as well as Solution B were diluted to 7.5 mM and frozen into a glasses at 77 K in EPR tubes equipped with a J. Young cap. Both EPR samples were photolyzed while constantly bathed in liquid nitrogen. Solution A changed from green to brown over the first 1 h, at which point the spectra shown in Figure 4 were collected. Solution B was treated as a control and exhibited a clean EPR spectrum corresponding to **1** that did not change upon prolonged photolysis side-by-side with Solution A. After photolyzing the solutions for 2 h, the solutions were allowed to stand at room temperature for 5 min before being frozen in liquid nitrogen once again. EPR spectra of both samples displayed complex **1** at this point. Solution A appeared bright red, consistent with the presence of highly colored TolN=NTol, which was confirmed by GC-MS. Solution B appeared light red-orange, consistent with the presence of **1**

and no exogenous TolN=NTol. Simulation parameters are listed in Table S4. A separate control was run with 7.5 mM N_3Tol and no Fe complex in solution. A weak signal similar to that previously reported for the free NTol nitrene[11] was observed in this case and did not align with the spectrum shown in Figure 4.

Table S4. EPR parameters implied from computer simulations of spectra

Complex	g_x	g_y	g_z	A_x (MHz)[a]	A_y (MHz)[a]	A_z (MHz)[a]
[SiP$^{iPr}_3$]Fe(N_2)	2.013	2.041	2.196	6.0	3.7	25.4
[SiP$^{iPr}_3$]Fe(η^1-N_3Ad)	2.013	2.036	2.210	6.7	6.5	0
[SiP$^{iPr}_3$]Fe(N_3Tol)	2.041	2.130	2.146	6.9	4.0	28.9
[SiP$^{iPr}_3$]Fe(NTol)	1.990	2.032	2.087	55	40	50

[a] *A* values correspond to hyperfine splitting from 3 equivalent I = 1/2 (i.e., phosphorus) nuclei, except in the case of [SiP$^{iPr}_3$]FeNTol, where only 1 P nucleus was included.

Competitive trapping experiments.

Reactions with *tert*-butylisocyanide. To solutions of **1** in C_6D_6 was added 1 equiv each of N_3Tol and ^{t}BuNC, resulting in a dark brown color. After stirring for 2 days at room temperature, the solutions had become red-colored. Analysis by ^{1}H NMR revealed the presence of the following products: TolN=NTol, ^{t}BuN=C=NTol, **1**, and **5**. The presence of **1** and **5** was also confirmed by IR spectroscopy of the solution. Characterization data for **5** matched that of a sample prepared independently from **1** and ^{t}BuNC (*vide supra*). The yields of azotoluene and carbodiimide were 29% and 15%, respectively. No TolNH_2 was observed. Under air, the solutions were filtered through silica gel and analyzed by GC-MS, confirming the presence of TolN=NTol and ^{t}BuN=C=NTol. The characterization data for ^{t}BuN=C=NTol matched that of authentic samples prepared by literature methods.[4]

Reactions with 9,10-dihydroanthracene. In a typical experiment, a C_6D_6 solution containing **1** and N_3Tol (1:1) was added to 0.5 equiv of 9,10-dihydroanthracene. After stirring for 18 h, the red solution was analyzed by ^{1}H NMR. Two paramagnetic products were evident: **1** and **6**. ^{1}H NMR data for **6** matched that of material synthesized independently from [SiP$^{iPr}_3$]Fe(OTf) and LiNHTol (*vide supra*). Three diamagnetic products were also evident (in addition to unreacted 9,10-dihydroanthracene): TolN=NTol, NH_2Tol, and anthracene. Under air, the solution was filtered through silica gel and analyzed by GC-MS, confirming the assignments of the diamagnetic components.

For utilization of GC-MS for quantitative measurements, calibration curves were made over the range 0-50 ppm with triphenylamine as an internal standard. These calibration curves are shown in Figure S8.

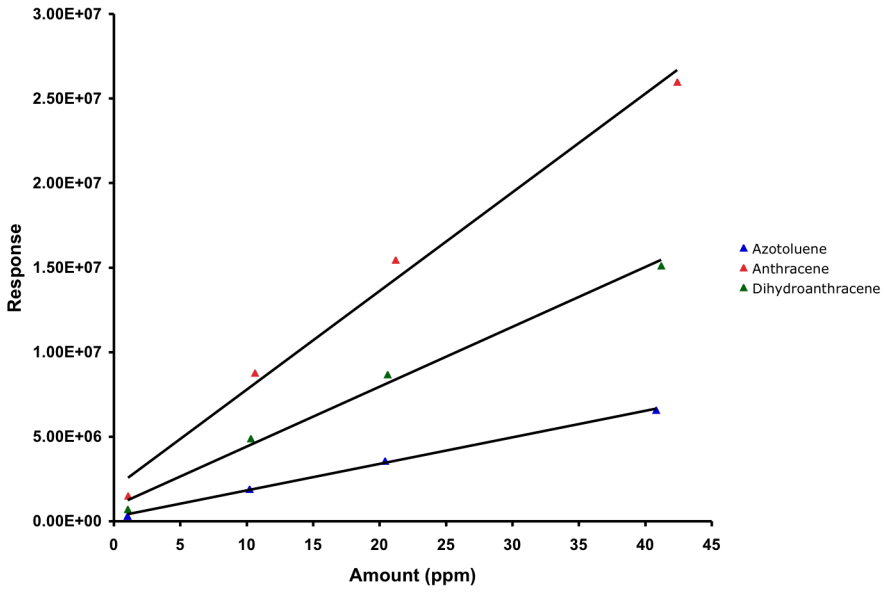

Figure S8. GC-MS calibration curves for azotoluene, anthracene, and 9,10-dihydroanthracene using triphenylamine as an internal standard.

Table S5 was constructed as follows. For Entries 1-3, a freshly prepared stock solution of **1** and N_3Tol was immediately added to various amounts of 9,10-dihydroanthracene. For Entries 4-6, a freshly prepared stock solution of N_3Tol and 9,10-dihydroanthracene was added to varying amounts of **1**. For Entries 7-12, a freshly prepared stock solution of **1** and 9,10-dihydroanthracene was split into three equal parts, and various amounts of N_3Tol were added to each one. (*Note*: Control experiments established that under analogous reaction conditions, no reactions are observed between 9,10-dihydroanthracene and either **1** or N_3Tol individually, and so the order of addition is not important.) For all Entries 1-12, the solutions were stirred for 18 h prior to opening them to the air, filtering them through silica gel, and analyzing them by GC-MS. A sample GC trace is shown in Figure S9. Concentrations of 9,10-dihydroanthracene, azotoluene, and anthracene were quantitated using the Agilent data analysis software and the calibration curves described above. Table S5 summarizes the results, and Figure S10 plots the azotoluene/anthracene ratio against Fe concentration, implying that two Fe centers are involved

in the N-N bond-forming step.

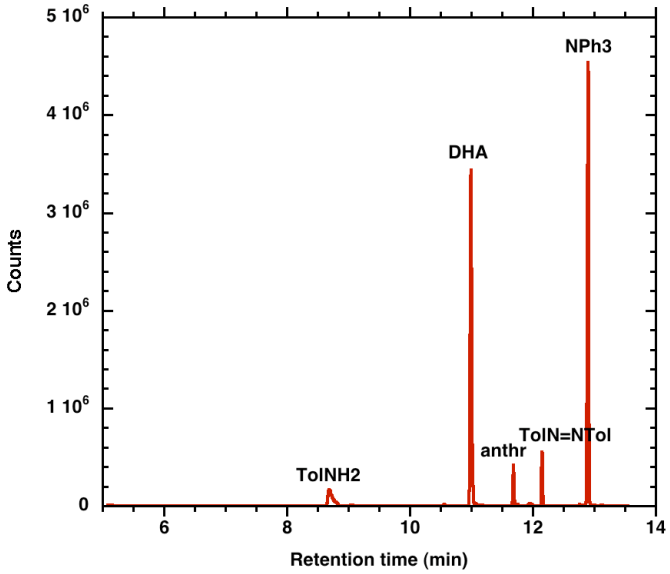

Figure S9. Sample GC trace (in this case from Table S5, Entry 4) showing the compounds quantitated and the internal standard (NPh_3).

Table S5. Analysis of product distributions resulting from varying the concentrations of individual reagents.

Entry	[Fe] (mM)	[TolN$_3$] (mM)	[DHA] (mM)	Product ratio (TolN=NTol/anthracene)
1	13.7	13.7	11	2.5
2	13.7	13.7	25	1.2
3	13.7	13.7	68.8	0.8
4	20.0	20.0	10	4.2
5	9.0	20.0	10	2.6
6	4.2	20.0	10	1.6
7	20.0	25.0	10	4.1
8	20.0	20.0	10	4.6
9	20.0	6.7	10	4.2
10	10.6	10.7	5.2	3.1
11	10.6	7.1	5.2	3.1
12	10.6	3.6	5.2	2.6

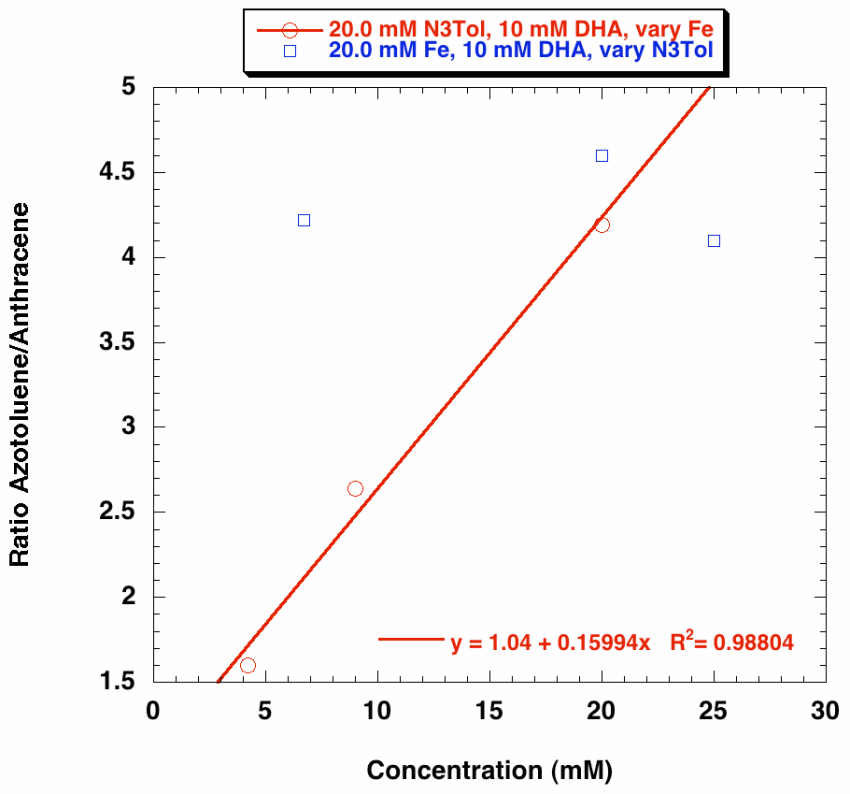

Figure S10. Plot of the azotoluene/anthracene ratio versus reagent concentration (as indicated in legend).

DFT Calculations.

Density functional calculations were carried out using the Gaussian03 suite[12] using the unrestricted B3LYP functional. For complexes **1** and **2**, the 6-311++G** basis set was utilized to do single-point energy calculations using crystallographic coordinates. Initial coordinates for **7** were generated by taking crystallographic coordinates of complex **6**, removing the N-H hydrogen, truncating the *p*-tolyl group to a phenyl group, and truncating the *iso*-propyl groups to methyl groups. The 6-31+G* basis set was used for obtaining minimized structures for **7-LS** and **7-IS**, and subsequently the final electronic structure calculations used the 6-311++G** basis set. Mülliken population analysis was used to examine spin density. The molecular orbital and spin density contour plots were generated using GaussView 4.1.[13] Frontier orbitals, spin density plots, optimized structures, and tabulated data are presented below.

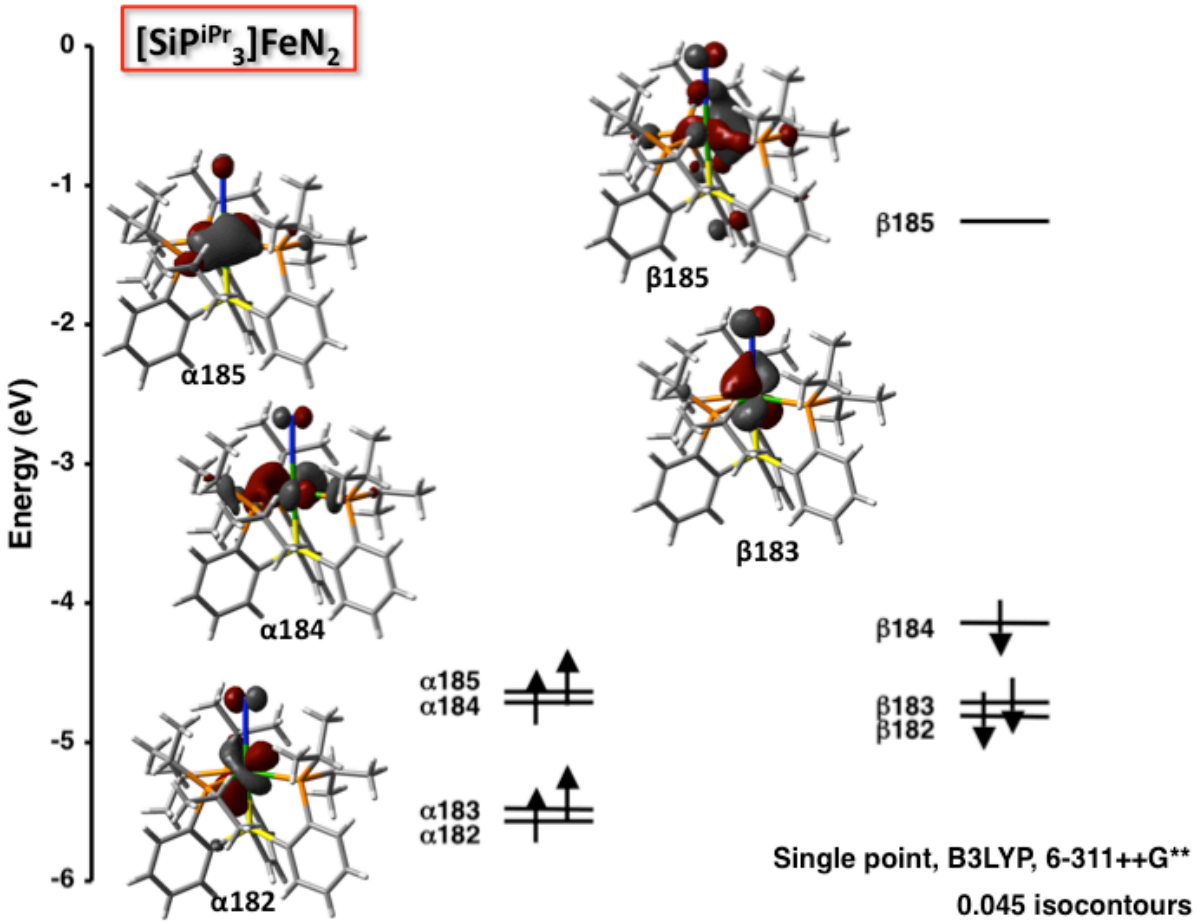

Figure S11. Frontier molecular orbitals of **1**.

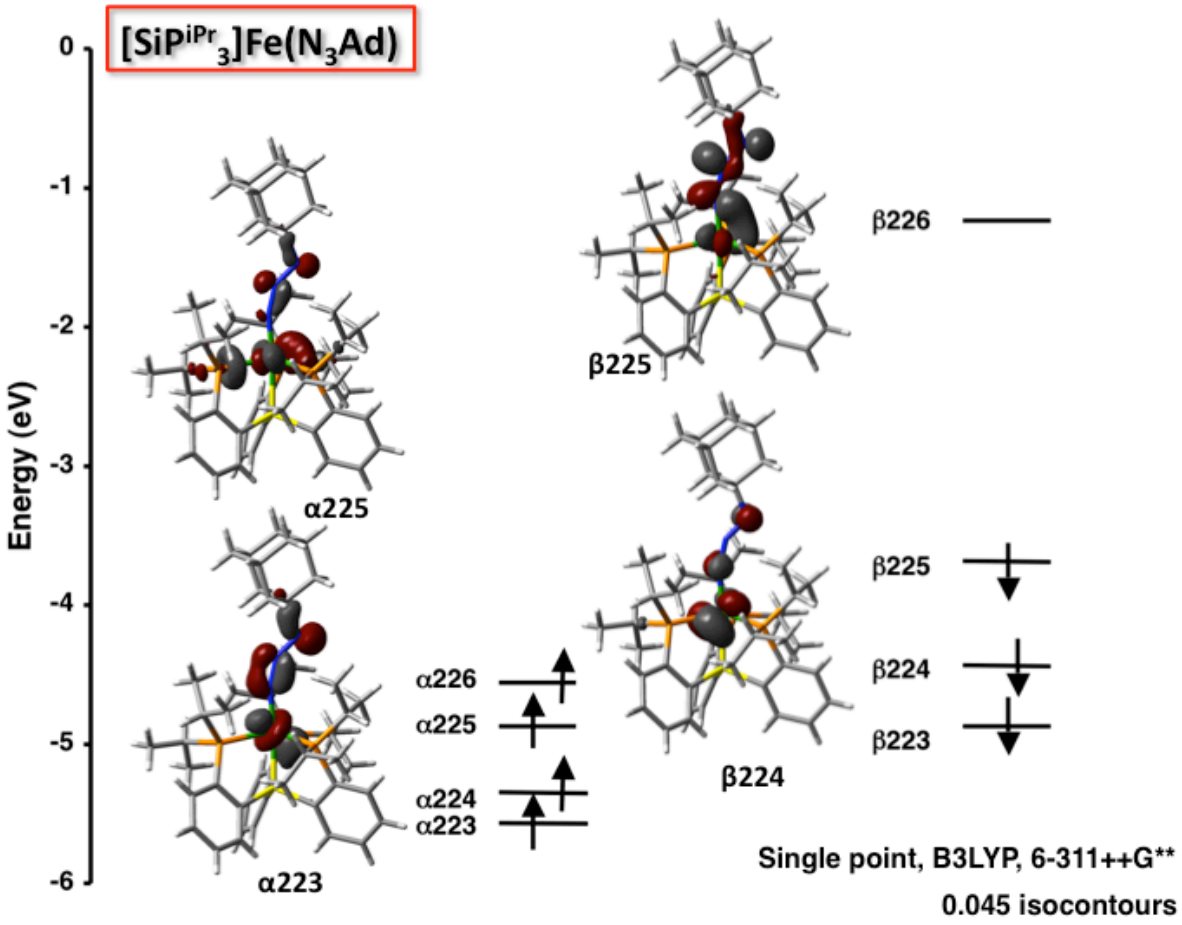

Figure S12. Frontier orbitals of **2**.

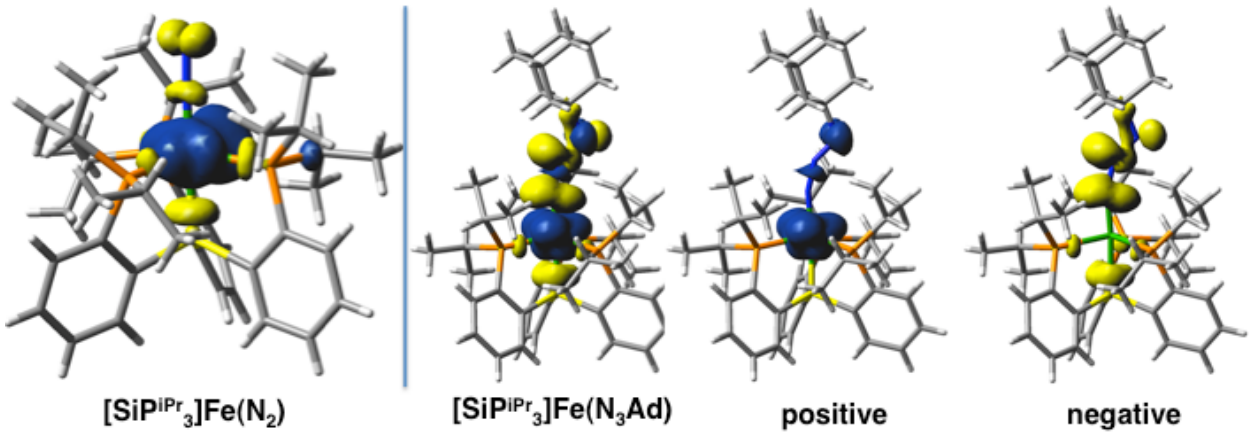

Figure S13. Spin density plots (0.002 isocontours). (*left*) Complex **1**. (*right*) Combined, positive phase, and negative phase spin density of **2**.

Table S6. Mülliken spin densities of complexes **1** and **2**.

Atom(s)	Spin density, [SiP$^{iPr}_3$]Fe(N$_2$)	Spin density, [SiP$^{iPr}_3$]Fe(N$_3$Ad)
Fe	0.92	1.59
N_α	0.03	-0.53
N_β	-0.09	-0.47
N_γ	N/A	0.23
P	0.01	0.22
Si	-0.01	-0.05
C,H	0.14	0.01
total	1.00	1.00

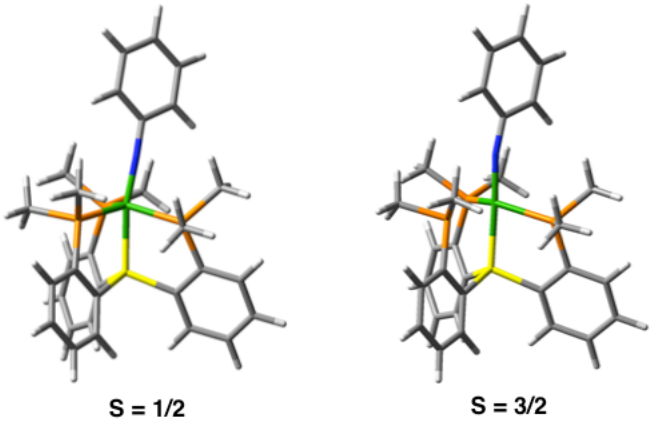

Figure S14. Optimized structures of [SiP$^{Me}_3$]Fe(NPh) (**7**): (*left*) low spin, **7-LS**; (*right*) intermediate spin, **7-IS**.

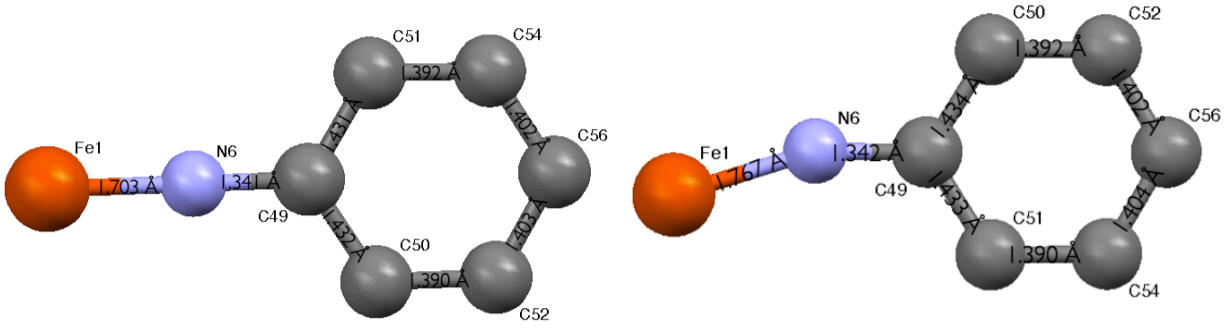

Figure S15. Bond lengths within the FeNPh groups of **7-LS** (*left*) and **7-IS** (*right*).

Table S7. Metric parameters for the optimized structures of **7-LS** and **7-IS**.

Metric	7-LS	7-IS
Fe-N (Å)	1.70322	1.76669
Fe-Si (Å)	2.35284	2.37279
Fe-P (Å)	2.21410, 2.27132, 2.24227	2.28779, 2.38238, 2.32360
N-C (Å)	1.34087	1.34208
P-Fe-P (deg)	107.41438, 134.78183, 109.26326	109.09305, 108.12322, 135.87987
Si-Fe-N (deg)	164.46463	177.82614
Fe-N-C (deg)	174.41771	161.98101
τ	0.49	0.70

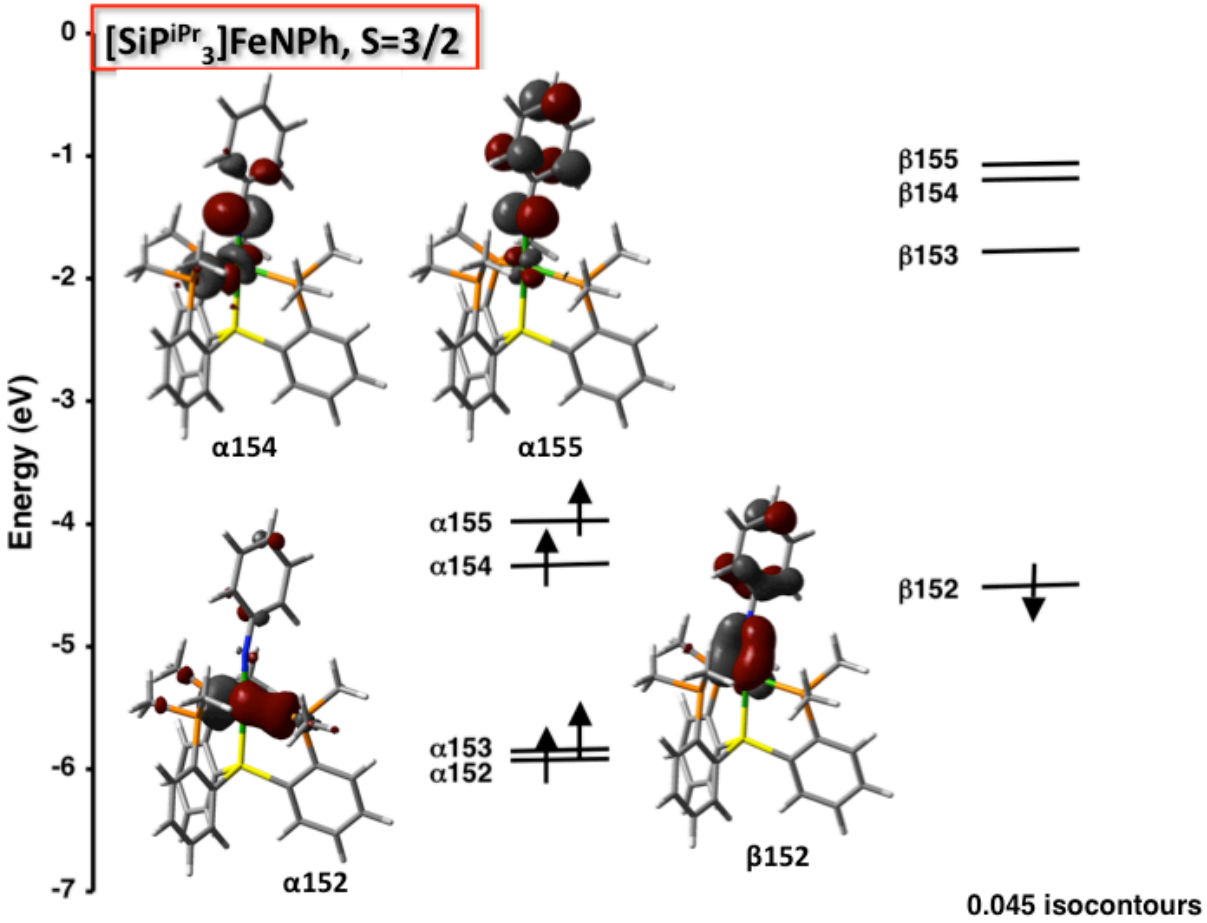

Figure S16. Frontier orbitals of **7-IS**.

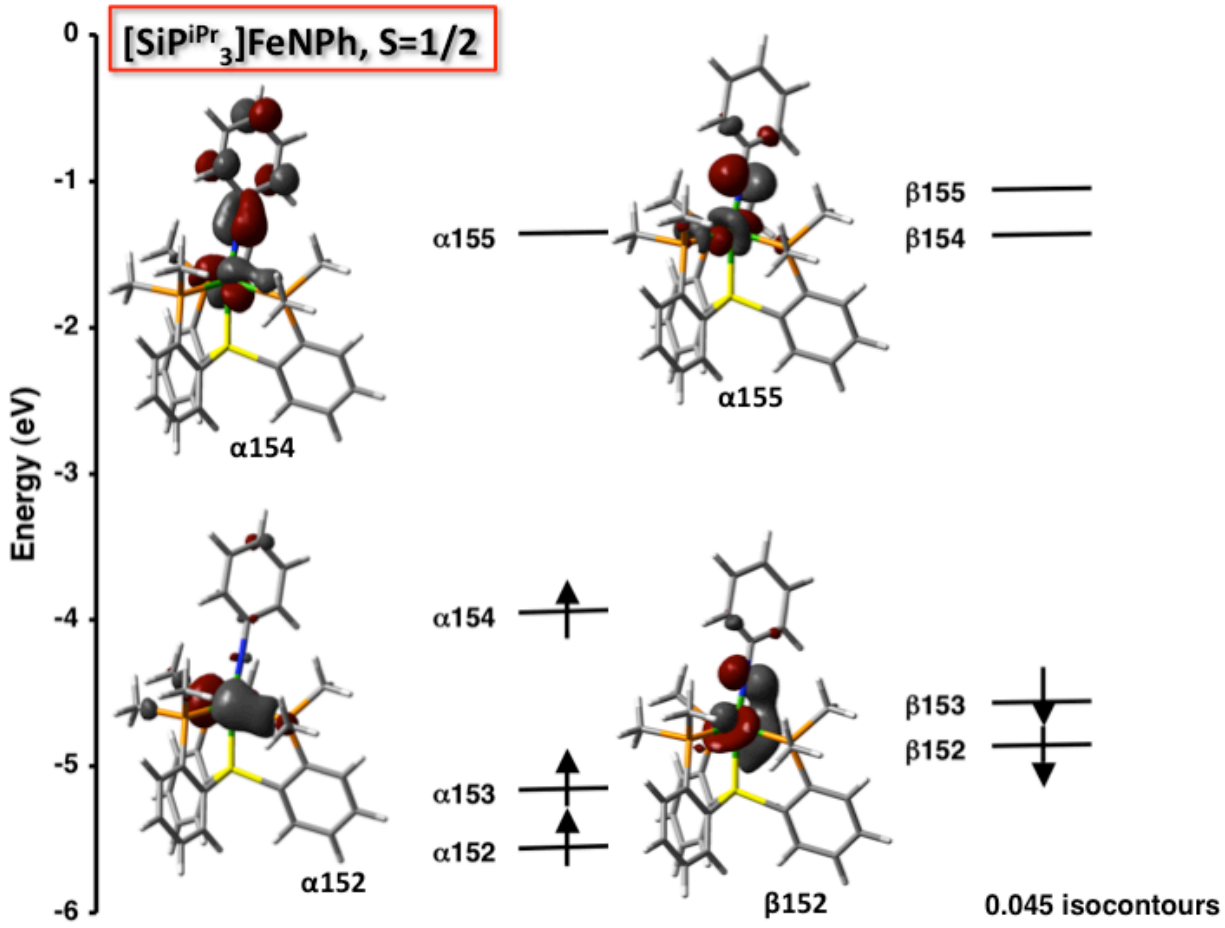

Figure S17. Frontier orbitals of **7-LS**.

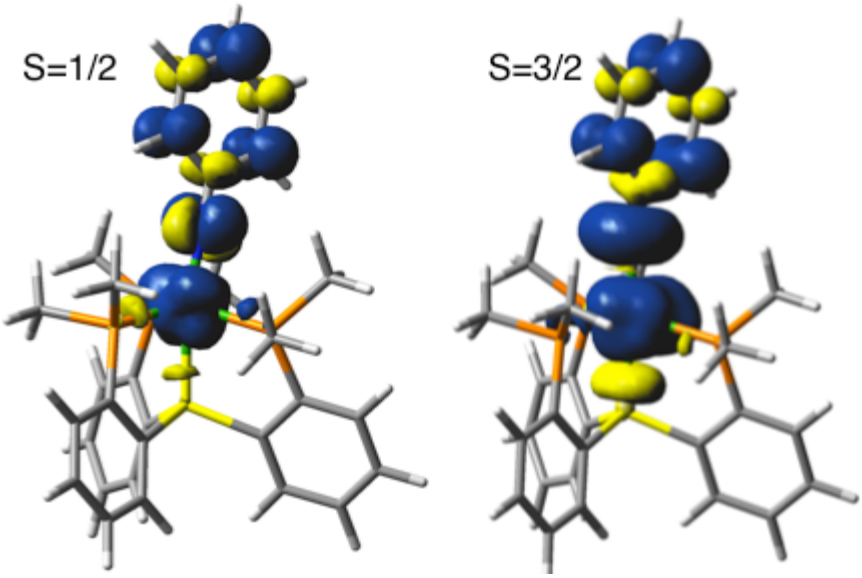

Figure S18. Spin density plots (0.002 isocontours) of (*left*) **7-LS** and (*left*) **7-IS**.

Table S8. Mülliken spin densities of complexes **7-LS** and **7-IS**.

Atom(s)	Spin density, 7-LS	Spin density, 7-IS
Fe	0.89	2.00
N	0.01	0.82
C,H (Ph)	0.15	0.15
P	-0.07	0.04
Si	-0.06	-0.18
C,H (SiP^{Me}_3)	0.08	0.17
total	1.00	3.00

Table S9. Crystal data and structure refinement for compound **2**.

Empirical formula	$C_{53.50}H_{87}FeN_3P_3Si$	
Formula weight	949.11	
Temperature	100(2) K	
Wavelength	0.71073 Å	
Crystal system	Rhombohedral	
Space group	*R*-3*c*	
Unit cell dimensions	*a* = 15.0449(8) Å	α = 90°
	b = 15.0449(8) Å	β = 90°
	c = 81.101(6) Å	γ = 120°
Volume	15897.8(17) $Å^3$	
Z	12	
Density (calculated)	1.190 Mg/m^3	
Absorption coefficient	0.435 mm^{-1}	
F(000)	6168	
Crystal size	0.50 x 0.50 x 0.45 mm^3	
Theta range for data collection	1.51 to 30.50°.	
Index ranges	$-21 \le h \le 21$, $-21 \le k \le 21$, $-115 \le l \le 115$	
Reflections collected	136582	
Independent reflections	5406 [R(int) = 0.0557]	
Completeness to theta = 30.50°	99.8 %	
Absorption correction	Semi-empirical from equivalents	
Max. and min. transmission	0.8284 and 0.8120	
Refinement method	Full-matrix least-squares on F^2	
Data / restraints / parameters	5406 / 331 / 336	
Goodness-of-fit on F^2	1.210	
Final R indices [I>2sigma(I)]	R1 = 0.0516, wR2 = 0.1168	
R indices (all data)	R1 = 0.0588, wR2 = 0.1200	
Largest diff. peak and hole	0.429 and -0.375 e.$Å^{-3}$	

Table S10. Crystal data and structure refinement for compound **6**.

Empirical formula	$C_{43}H_{62}FeNP_3Si$	
Formula weight	769.79	
Temperature	100(2) K	
Wavelength	0.71073 Å	
Crystal system	Orthorhombic	
Space group	$P2_12_12_1$	
Unit cell dimensions	a = 13.4209(18) Å	α = 90°
	b = 14.619(2) Å	β = 90°
	c = 21.192(3) Å	γ = 90°
Volume	4157.8(10) $Å^3$	
Z	4	
Density (calculated)	1.230 Mg/m^3	
Absorption coefficient	0.537 mm^{-1}	
F(000)	1648	
Crystal size	0.30 x 0.20 x 0.10 mm^3	
Theta range for data collection	1.69 to 30.03°.	
Index ranges	$-18 \le h \le 18$, $-20 \le k \le 20$, $-29 \le l \le 29$	
Reflections collected	93936	
Independent reflections	12149 [R(int) = 0.0903]	
Completeness to theta = 30.03°	100.0 %	
Absorption correction	Semi-empirical from equivalents	
Max. and min. transmission	0.9482 and 0.8555	
Refinement method	Full-matrix least-squares on F^2	
Data / restraints / parameters	12149 / 1 / 459	
Goodness-of-fit on F^2	1.011	
Final R indices [I>2sigma(I)]	R1 = 0.0419, wR2 = 0.0820	
R indices (all data)	R1 = 0.0587, wR2 = 0.0899	
Absolute structure parameter	-0.016(11)	
Largest diff. peak and hole	0.363 and -0.239 e.$Å^{-3}$	

References

[1] Mankad, N. P.; Whited, M. T.; Peters, J. C. *Angew. Chem., Int. Ed.* **2007**, *46*, 5768.

[2] Kitamura, Y.; Taniguchi, K.; Maegawa, T.; Monguchi, Y.; Kitade, Y.; Sajiki, H. *Heterocycles* **2009**, *77*, 521-532.

[3] For azoarenes: Lu, W.; Xi, C. *Tetrahdron Lett.* **2008**, *49*, 4011-4015.

[4] For carbodiimides: Ito, Y.; Hirao, T.; Saegusa, T. *J. Org. Chem.* **1975**, *40*, 2981-2982.

[5] Sheldrick, G. M. (1990). *Acta Cryst.* **A46**, 467-473.

[6] Sheldrick, G. M. (2008). *Acta Cryst.* **A64**, 112–122.

[7] Müller, P. *Crystallography Reviews* **2009**, *15*, 57-83.

[8] Evans, D. F. *J. Chem. Soc*, **1959**, 2003-2005.

[9] Sur, S. K. *J. Magn. Reson.* **1989**, **82**, 169-173.

[10] Neese, F. *QCPE Bull*. **1995**, *15*, 5.

[11] Hall, J. H.; Fargher, J. M.; Gisler, M. R. *J. Am. Chem. Soc*. **1978**, *100*, 2029.

[12] Frisch, M. J.; Trucks, G. W.; Schlegel, H. B.; Scuseria, G. E.; Robb, M. A.; Cheeseman, J. R.; Montgomery, J. A. J.; Vreven, T.; Kudin, K. N.; Burant, J. C.; Millam, J. M.; Iyengar, S. S.; Tomasi, J.; Barone, V.; Mennucci, B.; Cossi, M.; Scalmani, G.; Rega, N.; Petersson, G. A.; Nakatsuji, H.; Hada, M.; Ehara, M.; Toyota, K.; Fukuda, R.; Hasegawa, J.; Ishida, M.; Nakajima, T.; Honda, Y.; Kitao, O.; Nakai, H.; Klene, M.; Li, X.; Knox, J. E.; Hratchian, H. P.; Cross, J. B.; Adamo, C.; Jaramillo, J.; Gomperts, R.; Stratmann, R. E.; Yazyev, O.; Austin, A. J.; Cammi, R.; Pomelli, C.; Ochterski, J. W.; Ayala, P. Y.; Morokuma, K.; Voth, G. A.; Salvador, P.; Dannenberg, J. J.; Zakrzewski, V. G.; Dapprich, S.; Daniels, A. D.; Strain, M. C.; Farkas, O.; Malick, D. K.; Rabuck, A. D.; Raghavachari, K.; Foresman, J. B.; Ortiz, J. V.; Cui, Q.; Baboul, A. G.; Clifford, S.; Cioslowski, J.; Stefanov, B. B.; Liu, G.;

Liashenko, A.; Piskorz, P.; Komaromi, I.; Martin, R. L.; Fox, D. J.; Keith, T.; Al-Laham, M. A.; Peng, C. Y.; Nanayakkara, A.; Challacombe, M.; Gill, P. M. W.; Johnson, B.; Chen, W.; Wong, M. W.; Gonzalez, C.; Pople, J. A. Gaussian03, Rev. C02; Gaussian, Inc.: Pittsburgh PA, 2004.

[13] GaussView, Version 4.1; Roy Dennington II, Todd Keith and John Millam, Semichem, Inc., Shawnee Mission, KS, 2007.